Results in Materials 17 (2023) 100380

Contents lists available at ScienceDirect

Results in Materials

journal homepage: www.sciencedirect.com/journal/results-in-materials

Elastic deformation of thermal radiative and convective hybrid SWCNT-*Ag* and MWCNT-MoS_4 magneto-nanofluids flow in a cylinder

S.O. Salawu [a,*], A.M. Obalalu [b], E.O. Fatunmbi [c], MD Shamshuddin [d]

[a] Department of Mathematics, Bowen University, Iwo, Nigeria
[b] Department of Physics, Augustine University, Epe, Nigeria
[c] Department of Mathematics and Statistics, Federal Polytechnic, Ilaro, Nigeria
[d] Department of Mathematics, School of Sciences, SR University, Warangal, Telangana, India

ARTICLE INFO

Keywords:
Nanofluid hybridization
Thermal radiation
Elastic deformation
Heat propagation

ABSTRACT

An increasing interest in heat transfer of industrial working fluids and thermal applications of nanofluids propels the advancement of nanotechnology. Recently, focuses have been shifted to hybridization of nanofluids with the aim of enhancing heat propagation rate of conventional fluids. Hence, in this study, the elastic deformation of thermal radiation and convection for hybridized SWCNT-*Ag* and MWCNT-MoS_4 magneto-nanomaterials in engine oil is examined. The thermal transfer of the hybrid nanofluids occurs in a vertical cylinder with thermo-fluidic features being considered in the model formulation. With appropriate variables, an invariant transformation of the model is obtained, which is then solved using Chebyshev Collocation Scheme (CCS). The data outcomes revealed that heat distribution is reduced with rising Prandtl number, elastic deformation and the viscoelastic term for both SWCNT-Ag and MWCNT-MoS_4 hybrid nanofluids.

1. Introduction

The quest to improve the quality of life, energy saving, economic saving and product quality propels nanotechnology concept. Nanofluid serves as an important aspect of nanotechnology, which is useful in agriculture, chemical industry, electronics, pharmaceutical medicine and so on [1,2]. In general, nanofluids have good thermal conductivity characteristics than convectional liquid such as water, engine oil, kerosine, etc., Jamshed et al. [3]. To strengthen the thermal propagation performance of a traditional fluid, nanoparticles from nanofluid are dispersed in a suspension base fluid. Hence, the addition of metal oxide or solid metal particles of nanometer size in a base fluid raises the heat conductivity of the fluid, Ogunseye et al. [4]. As reported by Eastman et al. [5], 0.3% of copper nanoparticles enhanced enthylene-glycol fluid thermal conductivity by 40%. Das et al. [6] established that Al_2O_3 nanoparticles of 1–4% increased water based fluid heat conductivity by 10–25%. Gupta et al. [7] presented radiative and convective heat distribution of nanofluid hydromagnetic stagnation point flow and chemical reaction in a stretched inclined sheet. It was found that nanoparticles random motion, reduced or increased with respective rise in Brownian motion or thermophoresis term. Tadesse et al. [8] discussed the magnetized ferrofluid stagnation point flow along a stretching convectively heated plate with saturated permeable media. As seen, magnetized volume fraction nanoparticles heat transfer is encouraged, but resisted with rising porous term. Other view thermofluid terms effect on enhancing thermal conductivity of nanofluids can be obtained in Refs. [9–13]. However, experimental results have proven that higher thermal conductivity of nanofluids can be achieved when more than one nanoparticles are dispersed in working fluids.

The dispersion of two or more kinds of nanoparticles in base fluids gives rise to hybrid nanofluids. Hybridized nanofluids are characterized with higher heat distribution, molecules concentration density, diameter and thickness nanomaterial than a unitary nanofluid. This has numerous usages in biomedical, heat exchanger, nuclear systems, solar system, generator cooling and many more [14,15]. Hybrid nanofluids thermal conductivity has no specific model for its prediction. However, rising in the industrial demand of nanomaterials for an improved technological advancement has inspired many scientists to study different nanofluids. Afridi et al. [16] considered in a thin needle, the $Cu/Al_2O_3–H_2O$ hybrid nanofluid flow with dissipative irreversibility energy. It was observed that hybrid nanofluids produced high temperature distribution than regular nanofluid. Salawu et al. [17] examined heat conduction of hybrid ferromagnetic $H_2O–Fe_3O_4$ and $H_2O–Mn–ZnFe_2O_4$ in a spinning disk using Von Karman swirling flow. The radial velocity

* Corresponding author.
E-mail address: salawu.olakunle@bowen.edu.ng (S.O. Salawu).

https://doi.org/10.1016/j.rinma.2023.100380
Received 10 December 2022; Received in revised form 9 February 2023; Accepted 13 February 2023
Available online 17 February 2023

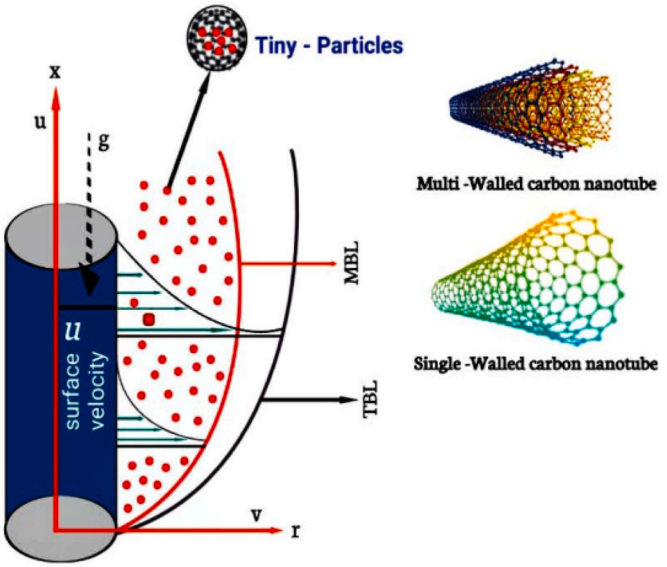

Fig. 1. Flow geometry description.

field was raised with increasing ferromagnetic interaction. Roy et al. [18] presented dissipation and radiation of composite nanofluid heat dispersion in an annular cylinder. The heat gradient was noticed to have increased with rising nanoparticle volume fraction. Khan et al. [19] numerically investigated the magnetized CNTs-ferrous oxide nanofluid flow in a channel. It was presented that 0.01–0.04% rise in the nanomaterial volume fraction raised the heat transfer from 1.7614 to 7.4413% and 1.6336–6.9519% for Fe_3O_4-MWCNTs and Fe_3O_4-SWCNTs respectively. Waqas et al. [20] studied thermal distribution of magnetized *Ag*-SWCNT and MoS_4-MWCNT hybrid nanoparticle interaction in a cylinder. Tiwari and Das nanoliquid formulation was considered, and temperature profile was found to have been raised with an increased temperature ratio. More valuable articles on hybrid nanoliquid can be seen in Refs. [21–24].

The essential of mixed convection and thermal radiation in maintaining heat transfer phenomenon of hybrid nanofluids cannot be overemphasized. The interesting applications of the thermophysical terms in nuclear reactor, solar collector, heat exchanger, atmospheric flows and others has fascinated scientists [11,25]. As such, Izadi et al. [26] discussed the convective hybrid ferrohydromagnetic nanoliquid in a porous saturated enclosure T-shape device. It was revealed that high convective heat distribution nanofluid was obtained with rising convective ratio between nanofluid and solid phases. Chamkha et al. [27] considered the flow of water-base hybrid nanoliquid with natural conjugate convection in a circular cavity. A high solid-liquid interface of thermal propagation of nanoparticles was observed. Zainal et al. [28] presented stagnation flow of mixed convective hybridized magneto-nanofluid along a convective vertical sheet. The volume fraction nanoparticle was seen to have increased the temperature distribution and the flow velocity was raised with an increasing mixed convection. Mandal and Shit [29] studied biviscosity of convective and radiative nanofluid heat transfer and entropy generation in a rotating stretchy disk. Observation revealed that the heat gradient and the skin friction was strongly influenced by nanoparticle size and thermal radiation. Fatunmbi et al. [12] examined temperature dependent properties of Casson nonlinear radiative nanofluid flow past an electromagnetic actuator. As noticed, temperature ratio and

Table 1
Thermofluidic properties values the hybrid nanoparticles and base liquid.

Properties	$\rho(kg/m^3)$	$k\ (W/mK)$	$C_p(J/kgK)$	$\sigma(S/m)$	$\beta \times 10^{-5}\ (1/K)$
Silver (*Ag*)	10,500	429	235	3.60×10^7	1.89
Molybdenum tetrasulfide (MoS_4)	5060	904.4	397.21	2.09×10^4	2.8424
Engine oil	884	0.1410	1910	$10^{-11} - 10^{-9}$	0.00007
SWCNTs	2600	6600	425	$10^{-6} - 10^{10}$	27
MWCNTs	1600	3000	796	10^6–10^7	44

radiation terms influenced the nanoparticle interaction, thereby increased heat transfer. Therefore, nanoparticles thermal propagation is highly supported by radiation and mixed convection increased.

This study aim to examine the elastic deformation of thermal convective and radiative hybrid SWCNT-*Ag* and MWCNT-MoS_4 magneto-nanofluids flow in a porous cylinder. In the study, enhancing thermal conductivity of stagnation flow of hybridized nanofluids is considered in the presence of porosity, nonlinear radiation, material elastic deformation, mixed convection, isothermal wall and magnetic field. Despite the usefulness of the study, the flow model has not been earlier posted and the flow characteristics has not been previously investigated. Various reports on the industrial applications and advancement of hybrid nanofluids motivated the investigation. Elastic deformation of materials is essentially used in ceramics, foam, plastic industry and many more. The mathematical model is solved by spectral based Chebyshev collocation technique, and the outcomes are presented in figures and tables. A qualitative discussion of the flow dynamical behaviour is accordingly presented.

2. Model description and development

Consider a thermal absorber and augmentation of mixed convective hybridized nanofluids flow influenced by electromagnetic force and gravity along a stretchy porous cylinder. An elastic deformation, viscous dissipation and varying radiation of the nanoparticle heat distribution is examined in an unbounded slip device. The dispersion of hybrid single walled carbon nanotube-silver (SWCNT-*Ag*) and multiple walls carbon nanotube-molybdenum tetrasulfide (MWCNT-MoS_4) nanoparticles is done in an engine oil base liquid. The *r*-axis is considered in the cylinder direction while the axial direction of the configuration is in *x*-axis as geometrically presented in Fig. 1. Without electric field polarization of the fluid material, the nanoparticles clustering is prevented by the surfactant of the particles. In modules, the controlling flow dimensional model based on the assumptions are as [30,31].

The controlling flow dimensional equations

$$\partial_r(vr) + \partial_x(ur) = 0, \tag{1}$$

$$u\partial_x(u) + v\partial_r(u) = U_s\frac{dU_s}{dx} + \nu_{hnf}\left(\frac{1}{r}\partial_r(u) + \partial_{rr}(u)\right) + \left(\frac{B_0^2\sigma_{hnf}}{\rho_{hnf}} + \frac{\nu_{hnf}}{K}\right)\left(U_s - u\right) + g\beta_T(T - T_b), \tag{2}$$

$$\left(\rho C_p\right)_{hnf}\left(u\partial_x(T)+v\partial_r(T)\right)=\frac{k_{hnf}}{r}\partial_r\left(r\partial_r(T)\right)+\frac{16\sigma_0}{3k_a}\frac{1}{r}\partial_r\left(rT^3\partial_r(T)\right)+\mu_{hnf}\left(\partial_r(u)\right)^2-\rho_{hnf}\beta k_e\left[\partial_r(u)\frac{1}{r}\partial_r\left(ru\partial_x(u)+rv\partial_r(u)\right)\right], \tag{3}$$

Following Nadeem et al. [32], the subjected boundary conditions are considered as:

$$u=\alpha\partial_r(u)+U_w(x),\ v=0,\ T=T_b,\ \text{at } r=R, \text{and } u\to U_s(x)=\frac{xU_0}{c},\ T\to T_\infty \text{ as } r\to\infty, \tag{4}$$

$$k_{hnf}\left(\partial_r(T)\right)_{r=R}=\nu(R,x)\rho_{hnf}[c_n(T_b-T_0)+\delta], \tag{5}$$

where the respective terms T temperature, T_b far stream temperature, T_0 wall temperature, U_s stretching velocity, u, v hybrid fluid velocity modules, U_w stretched surface velocity, k_{hnf} heat conductivity, U_0 free fluid flow velocity, R radius, ρ_{hnf} fluid density, c_n nanoliquid heat capacity, K permeability, c characteristic length, α latent heat, σ_{hnf} electric conductivity, q_a heat radiation, β_T heat expansivity coefficient, C_p specific heat, g gravity, B_0 magnetic strength, ν_{hnf} kinematic viscosity, β elastic deformation, σ_0 Stefan-Boltzmann and k_e elastic term.

As given by Refs. [33,34], the values of the effective thermophysical factors of the nanofluid in terms of the nanoparticles and engine oil base fluid is given in Table 1. Meanwhile, the thermofluidic description of the nanofluid variables are respectively expressed in Table 2. Whereas, the hybridized nanomaterial variables is demonstrated in Table 3.

To present the formulated mathematical equations in an invariant dynamically dimensionless form, the subsequent quantities are employed

$$\psi(\xi)=R\sqrt{U_w\nu_f}xf(\xi),\xi=\frac{r^2-R^2}{2R}\sqrt{\frac{U_0}{a\nu_f}},\theta(\xi)=\frac{T-T_b}{T_\infty-T_b},\ v=-\frac{R}{r}\sqrt{U_0\nu_f a}f(\xi),\ u=\frac{U_0x}{a}f'(\xi). \tag{6}$$

Employing the quantities in Eq. (6) on Eqs. (1)–(5), the dimensionless invariant equations are obtained as:

$$\frac{1}{h_1h_2}(2\lambda f_{\xi\xi}+(2\lambda\xi+1)f_{\xi\xi\xi})-(f_\xi)^2+ff_{\xi\xi}+\varepsilon^2+\left(\frac{1}{h_1h_2}Da+\frac{h_7}{h_6}M\right)(\varepsilon-f_\xi)+h_3\varphi\theta=0, \tag{7}$$

$$\frac{h_4}{Prh_5}(2\lambda\theta_\xi+(2\lambda\xi+1)\theta_{\xi\xi})+f\theta_\xi+\frac{Ra}{Prh_5}(\theta(\theta_a-1)+1)^2\Big[3(\theta_\xi)^2(2\lambda\xi+1)(\theta_a-1)+2\lambda\theta_\xi(\theta(\theta_a-1)+1)+\theta_{\xi\xi}(2\lambda\xi+1)(\theta(\theta_a-1)+1)\Big]-\frac{\beta\chi Ech_2}{h_1}\left[f_{\xi\xi}(f_\xi f_{\xi\xi}-ff_{\xi\xi\xi})\right]+\frac{Ech_5}{h_1}(2\lambda\xi+1)(f_{\xi\xi})^2=0, \tag{8}$$

the transformed invariant boundary conditions are

$$f_\xi(0)=1+\frac{\gamma}{h_1}f_{\xi\xi}(0),f_\xi(\infty)=\varepsilon,\theta(0)=0,\theta(\infty)=1,S(h_4)\theta_\xi(0)+Pr(h_2)f(0)=0, \tag{9}$$

Table 2
Nanofluid thermofluidic physical variables.

Variables	Nanofluid
Heat capacity	$(\rho C_p)_{nf}=(\rho C_p)_f\left(\psi\frac{(\rho C_p)_m}{(\rho C_p)_f}-\psi+1\right)$
Heat conduction	$\frac{k_{nf}}{k_f}=\frac{(m-1)k_f+k_m-\psi(m-1)(k_f-k_m)}{(m-1)k_f+k_m+\psi(k_f-k_m)}$
Viscosity	$\mu_{nf}=\frac{\mu_f}{(1-\psi)^{5/2}}$
Density	$\rho_{nf}=\rho_f\left[\psi\left(\frac{\rho_m}{\rho_f}\right)+(1-\psi)\right]$
Electrical conduction	$\frac{\sigma_{nf}}{\sigma_f}=\left[1+\frac{3\psi\left(\frac{\sigma_m}{\sigma_f}-1\right)}{\left(2+\frac{\sigma_m}{\sigma_f}\right)-\psi\left(\frac{\sigma_m}{\sigma_f}-1\right)}\right]$
Thermal expansion	$(\rho\beta_T)_{nf}=(\rho\beta_T)_f\left(1-\psi+\psi\frac{(\rho\beta_T)_m}{(\rho\beta_T)_f}\right)$

Table 3
Hybridized carbon nanotubes MoS_4–Ag nanofluid physical variables.

Variables	Hybrid nanofluids
Heat capacity	$(\rho C_p)_{hnf}=(\rho C_p)_f(1-\psi_2)\left[\psi_1\left(\frac{(\rho c_p)_{m1}}{(\rho c_p)_f}\right)+(1-\psi_1)\right]+\psi_2(\rho c_p)_{m2}$
Thermal conduction	$\frac{k_{hnf}}{k_{sf}}=\frac{(m-1)k_{sf}+k_{m2}-\psi_2(k_{sf}-k_{m2})(m-1)}{(m-1)k_{sf}+k_{m2}+\psi_2(k_{sf}-k_{m2})},\frac{k_{sf}}{k_f}=\frac{(m-1)k_f+k_{m1}-\psi_1(k_f-k_{m1})(m-1)}{(m-1)k_f+k_{m1}+\psi_1(k_f-k_{m1})}$
Viscosity	$\mu_{hnf}=\frac{\mu_f}{(1-\psi_2)^{5/2}(1-\psi_1)^{5/2}}$
Density	$\rho_{hnf}=\psi_2\rho_{m2}+\rho_f(1-\psi_2)\left[1-\varphi_1\left(\frac{\rho_{m1}}{\rho_f}\right)+\psi_1\right]$
electrical conduction	$\frac{\sigma_{hnf}}{\sigma_f}=\left[\frac{3\left(\frac{\psi_2\sigma_2+\psi_1\sigma_1}{\sigma_f}(\psi_2+\psi_1)\right)}{\left(2+\frac{\psi_2\sigma_2+\psi_1\sigma_1}{(\psi_2+\psi_1)\sigma_f}\right)-\left(\frac{\psi_2\sigma_2+\psi_1\sigma_1}{\sigma_f}(\psi_2+\psi_1)\right)}+1\right]$
Thermal expansion	$(\rho\beta_T)_{hnf}=(\rho\beta_T)_f(1-\psi)\left(1-\psi_1+\psi_1\frac{(\rho\beta_T)_{m1}}{(\rho\beta_T)_f}\right)+\psi_2(\rho\beta_T)_{m2}$

the resulting terms in Eqs. (7)–(9) are respectively the fluid curvature $\lambda = \sqrt{\frac{a\nu_f}{R^2U_0}}$, Porosity $Da = \frac{a\nu_f}{U_0K}$, magnetic term $M = \frac{\sigma_f B_0^2}{U_0\rho_f}$, stagnation term $\varepsilon = \frac{a}{c}$, Grashof number $Gr = \frac{g\beta_T x^2(T_b - T_\infty)}{\nu_f^2}$, mixed convection term $\varphi = \frac{Gr}{xRe^2}$, thermal radiation $Ra = \frac{16\sigma_0 T_\infty^3}{3k_f k_a}$, Eckert number $Ec = \frac{U_w^2}{(T_\infty - T_b)(C_p)_f}$, temperature ratio $\theta_a = \frac{T_\infty}{T_b}$, Prandtl number $Pr = \frac{\nu_f(\rho C_p)_f}{k_f}$, slip term $\gamma = \alpha(a\rho_f U_0)^{1/2}$, viscoelastic term $\chi = \frac{ak_e}{\nu_f}$ and designate factors (h_1, h_2, h_3, h_4, h_5, h_6 & h_7). The h_i, $i = 1, 2...7$ is defined as:

$$h_1 = (1-\psi_1)^{2.5}(1-\psi_2)^{2.5},$$

$$h_2 = \frac{\psi_2(\rho_{m2})}{\rho_f} + (1-\psi_2)\left(\frac{\rho_{m1}}{\rho_f}\psi_1 + (1-\psi_1)\right),$$

$$h_3 = \frac{\frac{\rho_{m2}\beta_{m2}}{\rho_f\beta_f}\psi_2 + (1-\psi_2)\left(\frac{\rho_{m1}\beta_{m1}}{\rho_f\beta_f}\psi_1 + (1-\psi_1)\right)}{\frac{\rho_{m2}}{\rho_f}\psi_2 + (1-\psi_2)\left(\frac{\rho_{m1}}{\rho_f}\psi_1 + (1-\psi_1)\right)},$$

$$h_4 = \frac{k_{m1} - \psi_1(m-1)(k_f - k_{m1}) + (m-1)k_f}{\psi_1(k_f - k_{m1}) + (m-1)k_f + k_{m1}} \cdot \frac{k_{m2} - \psi_2(m-1)(k_{sf} - k_{m2}) + (m-1)k_{sf}}{\psi_2(k_{sf} - k_{m2}) + (m-1)k_{sf} + k_{m2}},$$

$$h_5 = \frac{\rho_{m2}(C_p)_{m2}}{\rho_f(C_P)_f}\psi_2 + (1-\psi_2)\left(\frac{\rho_{m1}(C_p)_{m1}}{\rho_f(C_p)_f}\psi_1 + (1-\psi_1)\right),$$

$$h_6 = \frac{\rho_{m2}}{\rho_f}\psi_2 + (1-\psi_2)\left(\frac{\rho_{m1}}{\rho_f}\psi_1 + (1-\psi_1)\right),$$

$$h_7 = \sigma_f \left[1 + \frac{3\psi_1(m-1)\left(\frac{\sigma_{p1}}{\sigma_f} - 1\right)}{\left(2 + \frac{\sigma_{p1}}{\sigma_f}\right) - (m-1)\psi_1\left(\frac{\sigma_{p1}}{\sigma_f} - 1\right)} + \frac{3\psi_2(m-1)\left(\frac{\sigma_{p2}}{\sigma_f} - 1\right)}{\left(2 + \frac{\sigma_{p2}}{\sigma_f}\right) - (m-1)\psi_2\left(\frac{\sigma_{p2}}{\sigma_f} - 1\right)}\right].$$

2.1. Quantities of physical interest

The quantities of interest are the heat gradient and the skin drag force, which are described as:

$$Nu_x = \frac{q_b x}{(T_b - T_\infty)} \quad \text{and} \quad Cf_x = \frac{2\tau_b}{U_0^2\rho_f}. \tag{10}$$

The shear stress τ_b and heat flux q_b at the wall takes the form

$$\tau_b = \mu_{hnf}\partial_r(u)\big|_{r=R} \quad \text{and} \quad q_b = (q_r)_w - k_{hnf}\partial_r(T)\big|_{r=R}. \tag{11}$$

Substitute in Eqs. (6) and (11) in Eq. (10), then Eq. (10) becomes

$$Cf_x Re^{1/2} = \frac{1}{h_1} f_{\xi\xi}(0) \quad \text{and} \quad Nu_x Re^{-1/2} = -(h_4 + Ra(\theta(0)(\theta_a - 1) + 1)^3)\theta_\xi(0), \tag{12}$$

where Reynolds number $\mathrm{Re} = \frac{xU_0}{\nu_f}$.

3. Solution procedures

3.1. A summary of the Chebyshev collocation schemes (CCS)

The elastic deformation equations were solved using the CCS. For its global perspective and effectiveness in solving partial differential equations, ordinary differential equations, linear and nonlinear equations, the CCS basis functions are used in the solutions of the governing ordinary differential equation as adopted by Obalalu [35]. To make sure that the controlling ordinary differential equation is correct, the coefficients are arranged in a certain order. In order to generate residuals or errors, the predicted solutions are incorporated into the governing equations for the unknown dependent functions in the differential equations. The assumed CCS solutions with unknown coefficients were introduced. Also, by using the collocation method, the errors are then reduced to zero. A system of algebraic equations is built and then solved to get the values of the unknown coefficients.

3.2. Application of Chebyshev collocation schemes

Unknown functions $f(\xi)$ and $\theta(\xi)$ are considered to be solved by adding the Chebyshev base functions.

Table 4
CCM solutions in various approximation orders of Convergence when $\lambda = 0.2$, $M = 2$, $\varphi = 0.02$, $\theta_a = 1.1$, $\varepsilon = 0.2$, $Da = 0.9$, Pr = 3, $Ra = 0.8$, $Ec = 0.02$, $\gamma = 0.1$, $S = 0.2$, $\chi = 0.5$, $\beta = 1.0$

Number of iteration (N)	f_ξ	θ_ξ
4	1.035916	2.71253
6	1.004772	2.53722
8	1.003268	2.34009
10	1.002291	2.23211
12	1.002291	2.11111
14	1.002291	2.11111
16	1.002291	2.11111
20	1.002291	2.11111
24	1.002291	2.11111
30	1.002291	2.11111

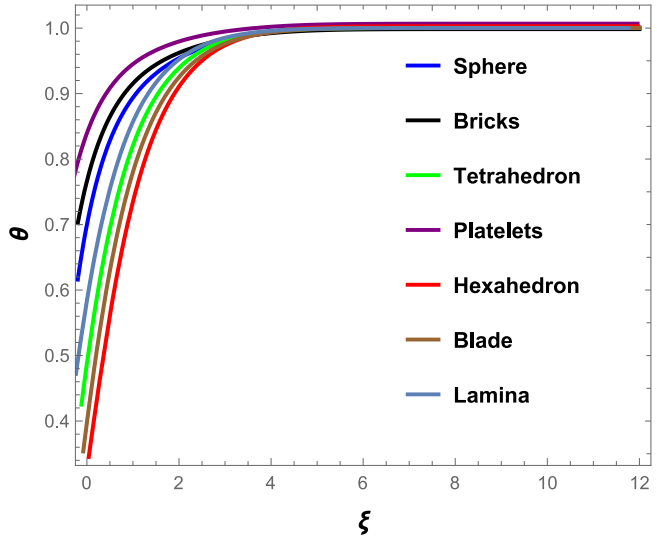

Fig. 2. Temperature profile for shape factors (single).

Table 5
Comparison of the heat gradient with Unyong et al. [36] and Kameswaran et al. [37] when $\lambda = M = 2 = \varphi = \theta_a = \varepsilon = Da = Ra = Ec = \gamma = S = \chi = \beta = 0$.

Pr	current work	Unyong et al. [36]	Kameswaran et al. [37]
0.72	1.08852	1.08852	1.08852
1.0	1.33333	1.3333	1.33333
3.0	2.50973	2.50973	2.50973
10.0	4.79687	4.79687	4.79687
100.0	15.71163	15.71163	15.71163

$$f(\xi) = \sum_{j=0}^{N} a_i U_j\left(\frac{2\xi}{L} - 1\right), \text{and } \theta(\xi) = \sum_{j=0}^{N} b_i U_j\left(\frac{2\xi}{L} - 1\right), \tag{13}$$

where a_i and b_i are unknown constant coefficients and scale parameter L denoted the boundary layer for the effective numerical computation. Using the domain truncation method, the problem domain is shifted from $[-1, 1]$ to $[0, L]$. Furthermore, in order to calculate the unknown coefficients, equation (13) is substituted and used on the boundary conditions in equation (9). In addition, $R_f(\xi, a_i, b_i)$ and $R_\theta(\xi, a_i, b_i)$ are the residuals obtained by inserting equation (13) into Eqs. (7) and (8). The collocation technique is used to reduce residues to the maximum degree of possibility.

$$\text{for } \hbar(\xi - \xi_j) = \begin{cases} 1, & \xi = \xi_j \\ 0, & \text{otherwise,} \end{cases}$$

$$\int_0^L R_f \hbar(\xi - \xi_j) d\xi = R_f(\xi_j, a_i) = 0, \quad \text{for } j = 1,\ 2, ..N - 1, \tag{14}$$

$$\int_0^L R_\theta \hbar(\xi - \xi_j) d\xi = R_\theta(\xi_j, a_i, b_i) = 0, \quad \text{for } j = 1,\ 2, ..N - 1. \tag{15}$$

The transformed CCS (shifted Gauss-Lobatto points) that were employed are:

$$\xi_j = \frac{1}{2}\left(1 - cos\left(\frac{j\pi}{N}\right)\right). \tag{16}$$

The algebraic equations with $2\ N\ +\ 2$ unknown constants are generated by Eqs. (14) and (15). With the help of MATHEMATICA 11.3, a mathematical symbolic program, the obtained equations are solved using the Newton approach. Due to the fast convergence of approximations and the ability to solve extremely non-linear systems of equations, the CCS based on spectral techniques was determined to be adequate and effective for achieving an approximate solution. The different approximation orders of convergence of the solution techniques are shown in Table 4. The square residual error produced by equations (14) and (15) are calculated and reported. Fig. 2 depicts the temperature profile for different shape factors (Lamina, Blade, Hexahedron, Platelets, Tetrahedron, Bricks and Sphere) of nanoparticles.

4. Results discussion

In this section, the parameters considered in this problem are given numerical values as follows: $\lambda = 0.2$, $M = 2$, $\varphi = 0.02$, $\theta_a = 1.1$, $\varepsilon = 0.2$, $Da = 0.9$, $\Pr = 3$, $Ra = 0.8$, $Ec = 0.02$, $\gamma = 0.1$, $S = 0.2$, $\chi = 0.5$, $\beta = 1.0$, unless specifically stated on the graphs or tables. A comparison of heat gradient Nu_x with previously published results is shown in Table 5. The current results for hybridized nanofluid are in great agreement with earlier investigations under limiting cases.

4.1. Parametric effects on the quantities of engineering interest

Table 6 specifically shows the reactions of the skin friction coefficient $Cf_xRe^{1/2}$ and the Nusselt number $NuRe^{-1/2}$ for both hybridized nanofluid $SWCNT - Ag$ and $MWCNT - MoS4$ for variations in some chosen physical parameters (γ, M, Ra, φ, Da&Ec). Evidently, an increase in the slip term γ (1.0, 1.5, 2.0) reduces $MWCNT - MoS4/Cf_xRe^{1/2}$ by

Table 6
Values of heat gradient and the skin drag force for MWCNT and SWCNT.

Parameter γ	M	Ra	φ	Da	Ec	MWCNT $Cf_xRe^{1/2}$	MWCNT $Nu_xRe^{-1/2}$	SWCNT $Cf_xRe^{1/2}$	SWCNT $Nu_xRe^{-1/2}$
1.0						1.9743	1.8143	2.2551	3.1241
1.5						1.8321	1.8008	2.1300	2.2679
2.0						1.7501	1.7909	2.0123	2.1031
	1.5					1.7199	2.4322	3.3211	3.6747
	2.0					1.6643	2.4113	3.2522	3.5531
	2.5					1.5521	1.9918	2.1321	3.2422
		0.5				1.2346	1.9730	2.5511	1.6130
		1.0				1.3213	1.8178	2.5218	2.1233
		1.5				1.4325	1.7990	3.4205	2.5765
			0.4			1.5302	1.8990	2.6743	3.6532
			0.6			1.7474	1.9102	2.8784	3.7943
			1.8			1.9435	1.9833	3.1772	3.8234
				1.9		1.2353	2.1632	2.5423	3.4522
				2.3		2.7545	2.0456	2.3463	3.5561
				2.7		2.2954	2.0115	2.2523	3.8189
					1.1	1.4255	1.7991	2.4457	3.2722
					1.7	1.6211	1.7991	2.5821	3.4898
					2.5	1.7491	1.7991	2.6532	3.6441

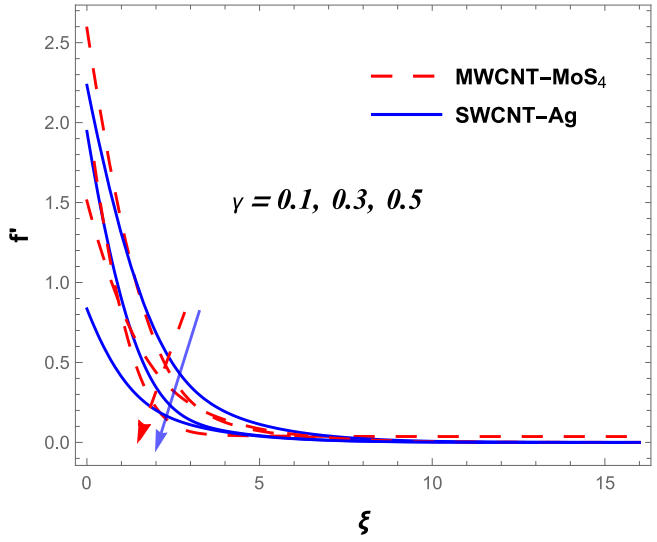

Fig. 3. Velocity field response to various γ

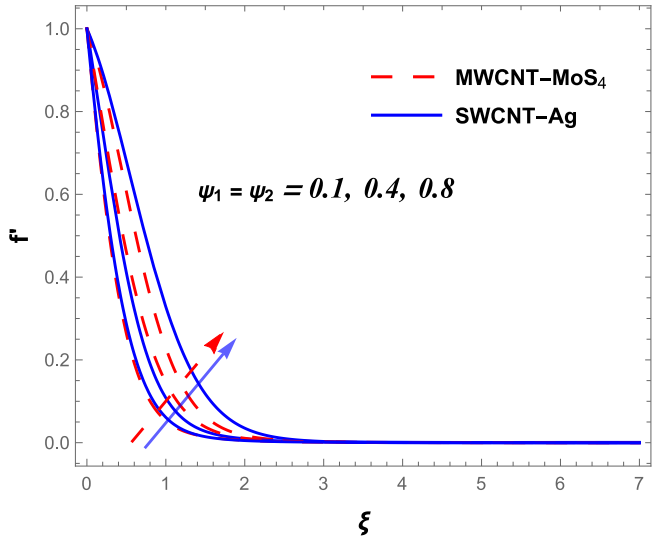

Fig. 4. Reaction of flow rate to rising ψ

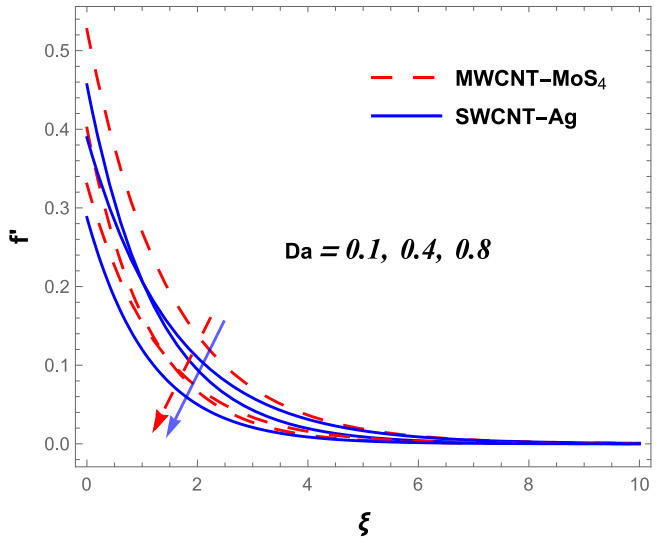

Fig. 5. Rising effect of *Da* on velocity field.

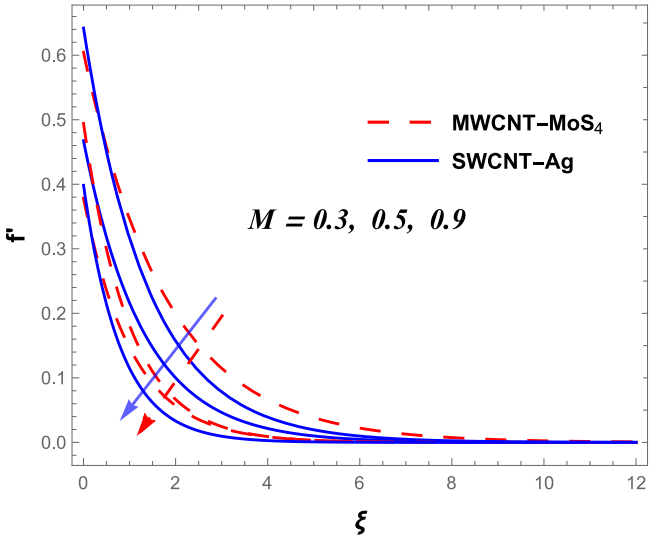

Fig. 6. Effect of M on flow rate field.

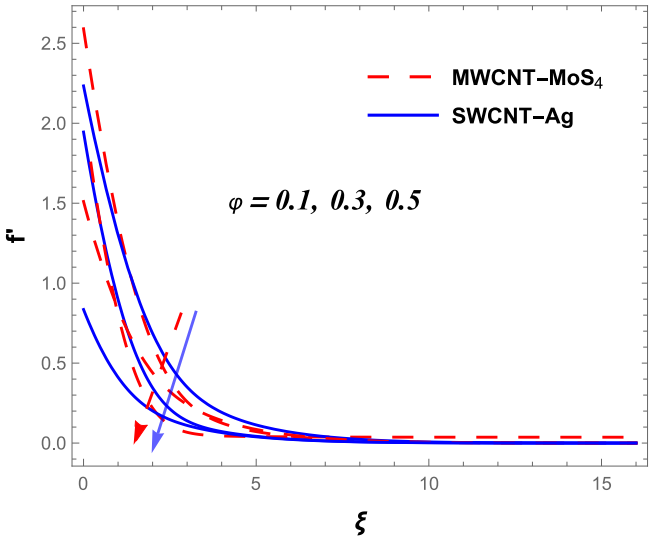

Fig. 7. Rising effect of φ on velocity field.

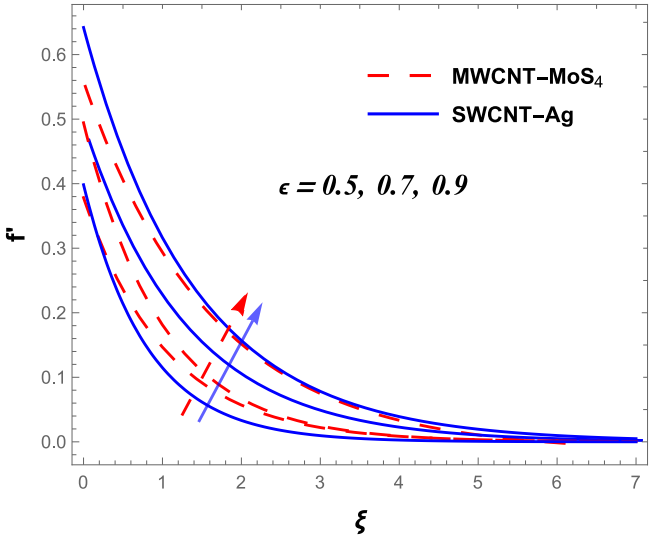

Fig. 8. Effect of ε on flow rate field.

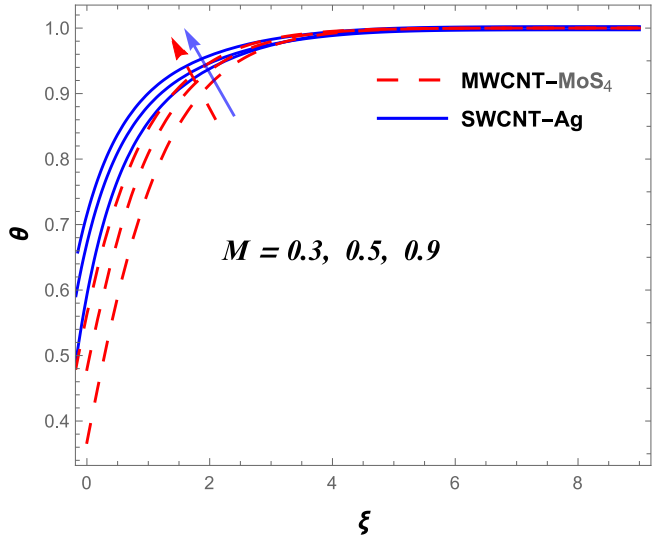

Fig. 9. Effect of rising M on thermal energy.

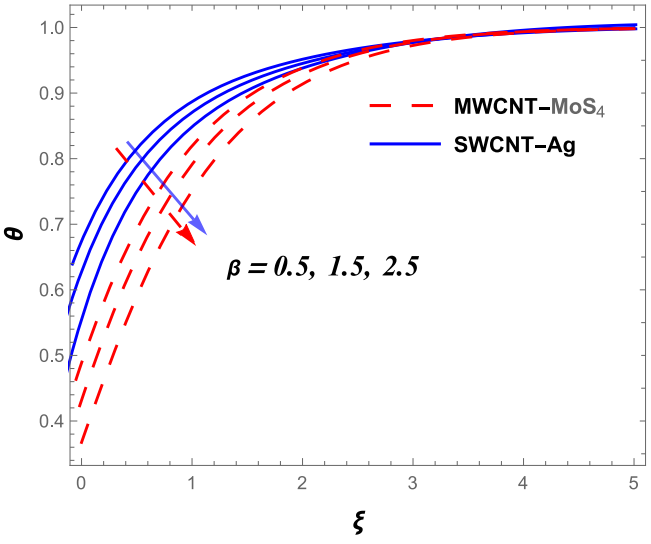

Fig. 11. Heat distribution for different β

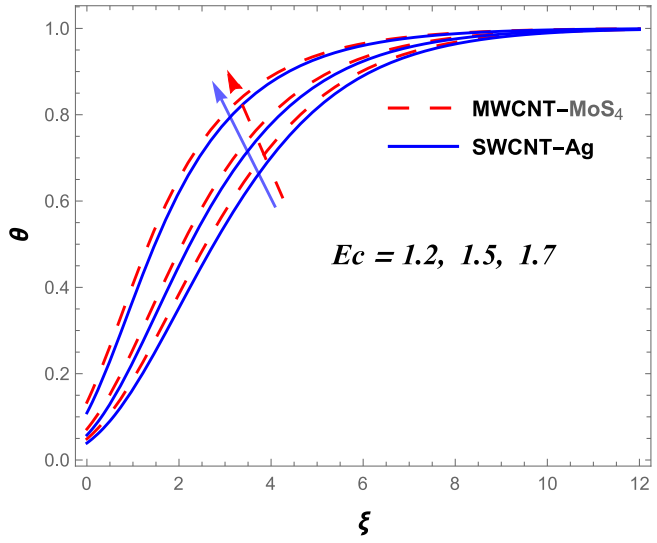

Fig. 10. Temperature field for rising Ec.

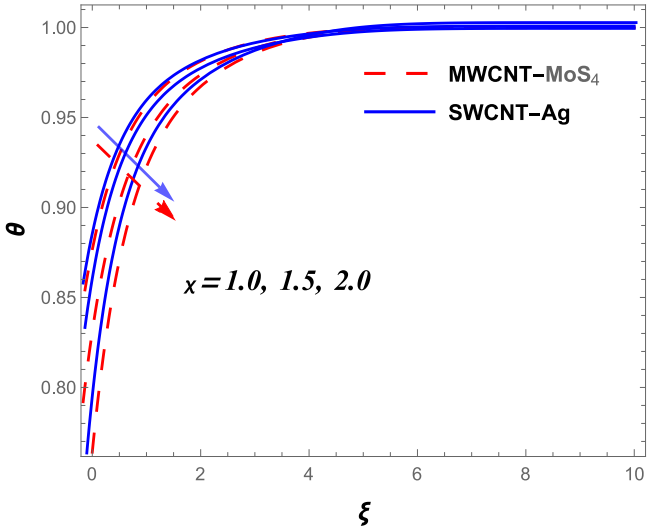

Fig. 12. Effect of χ on heat profile.

11.4% while $SWCNT-MoS4/Cf_xRe^{1/2}$ decreases by 10.8%. A rise in the magnetic field term M (1.5, 2.0, 2.5) also causes $MWCNT-MoS4/Cf_xRe^{1/2}$ to fall by 9.8% compared to a decrease of 35.8% in $SWCNT-MoS4/Cf_xRe^{1/2}$. The trend is however reversed for a rise in the Eckert number Ec and the mixed convection term φ as shown in the table. The engine oil base $MWCNT-MoS4/Cf_xRe^{1/2}$ rises by 22.7% (27.0%) as Ec (φ) increases while $SWCNT-MoS4/Cf_xRe^{1/2}$ increases by 8.5% (18.8%) respectively. Meanwhile, escalating values of Darcy term Da significantly raise the $Cf_xRe^{1/2}$ by 85.5% for $MWCNT-MoS4$ whereas $Cf_xRe^{1/2}/SWCNT-Ag$ declines by 11.4% with growth in Da. A rise in the magnitude of φ (0.4, 0.6,1.8) propels an improvement in the heat transfer $(Nu_{\mathrm{Re}}^{-1/2})$ for both hybridized nanofluid $MWCNT-Ag$ and $SWCNT-MoS4$. Furthermore, the Nusselt number $NuRe^{-1/2}$ (relating to surface heat transfer) for the $SWCNT-MoS4$ improves significantly by 59.7% increase with escalating values of the thermal radiation term Ra (0.5, 1.0, 1.5). Conversely, the engine oil base $SWCNT-MoS4$ hybridized nanofluid reduces by 8.8% as Ra rises. The heat transfer also depreciates by 18.1% for the $MWCNT-MoS4$ hybridized nanofluid with a rise in M whereas a decrease of 11.8% is encountered in the $SWCNT-MoS4$ hybridized nanofluid as M increases (1.5, 2.0, 2.5).

4.2. Parametric effects on the flow velocity distribution

The offered graphs in Figs. 3–8 demonstrate the structure of the hydrodynamic boundary layer and the trend of velocity profiles for variations in some chosen parameters for both hybridized nanofluid SWCNT-Ag and MWCNT-MoS_4. As visualized in Fig. 3, the fluid motion decelerates due to escalation in the magnitude of the slip term γ (0.1, 0.3, 0.5). Here, augmenting values of γ compels an unequal flow speed at the stretching surface and near the sheet. Consequent upon a rise in γ, a decline in the hydrodynamic boundary layer occurs in the presence of γ since the momentum induced at the stretching wall is partly transmitted to the hybridized nanofluid. However, the velocity profile for the engine oil base hybridized nanofluid SWCNT-Ag is lower as compared to MWCNT-MoS_4. The velocity profile enhances as the volume fractions of nano tiny particles ψ_1 and ψ_2 are raised as sketched in Fig. 4. Higher magnitudes of ψ_1 and ψ_2 accelerate the fluid motion for both hybridized nanofluid SWCNT-Ag and MWCNT-MoS_4. On the other hand, fluid movement is impeded by growth in the porosity term Da as found in Fig. 5. An enhancement in Da creates a resistance to the free motion of the fluid which causes the velocity profile to be declined. In Figs. 6 and 7, the impact of the magnetic field M and φ on the velocity profile is

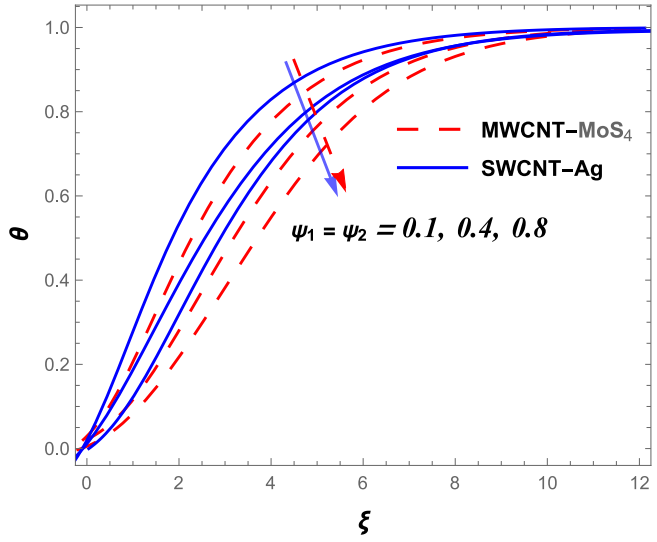

Fig. 13. Heat profile for various ψ

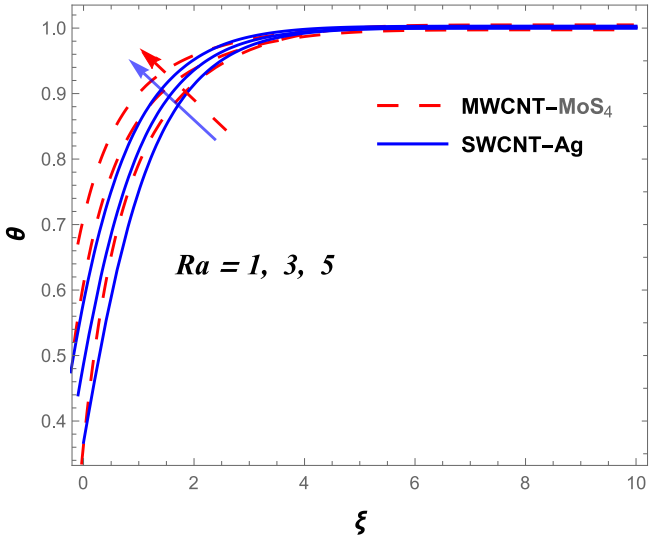

Fig. 15. Impact of rising *Ra* on heat profile.

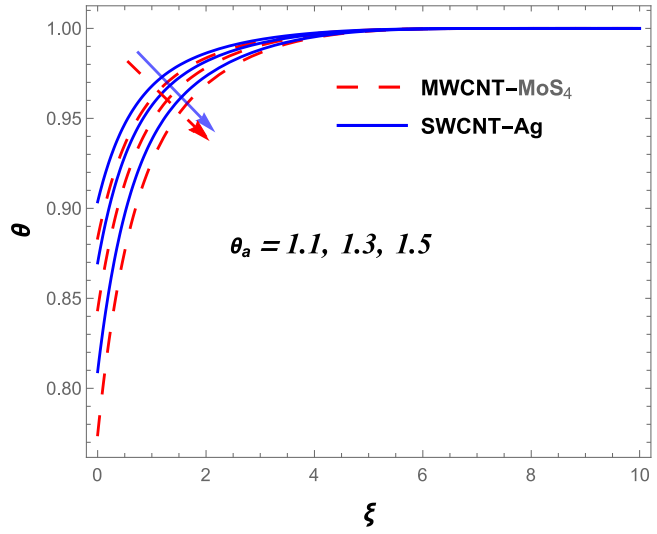

Fig. 14. Temperature field for θ_a.

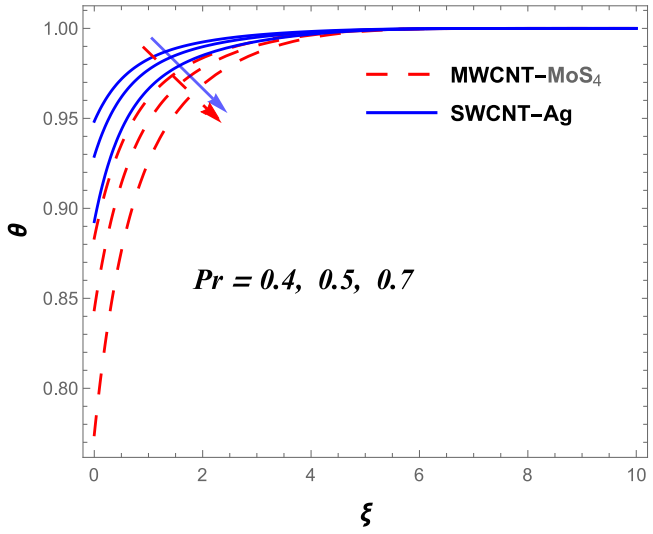

Fig. 16. Temperature profile for *Pr*.

respectively exposed for the engine oil base hybridized nanofluid SWCNT-*Ag* and MWCNT-MoS_4. Fig. 8 has been sketched to demonstrate how an increase in the stagnation term ε impacted on the motion of the fluid. It is found that the velocity profile uplifts as the magnitude of ε rises due to the direct proportionality of ε to the wall stretching rate a. With a rise in ε, the wall stretching rate a becomes higher than that of the upstream stretching rate, thus the velocity profile is uplifted.

4.3. Temperature field for various rising parameter values

The plots displayed in Figs. 9–16 elucidate the reaction of the thermal field to variations in some chosen parameters. Higher magnitude of M raises the thermal boundary layer structure for both SWCNT-*Ag* and MWCNT-MoS_4 as plotted in Fig. 9. The resistance created to the motion of fluid due to Lorentz force generates friction thereby creating extra heat in the fluid and consequently boost the temperature. Likewise, Fig. 10 reveals that the temperature distribution increases as the Eckert number *Ec* rises. A hike in *Ec* creates a frictional heating owing to viscous dissipation. Conversely, an increase in the elastic deformation term β and the viscoelastic term χ shrink the thermal boundary layer and consequently lower the surface temperature as respectively visualized in Figs. 11 and 12. The reaction of the heat distribution profile for variations in the volume fractions ψ_1 and ψ_2 is sketched in Fig. 13. In this graph, the temperature shows a downward trend for increasing values ψ_1 and ψ_2 for both SWCNT-*Ag* and MWCNT-MoS_4. A rise in the temperature ratio term θ_a causes the thermal boundary layer structure field to depreciate and reduce the surface temperature for SWCNT-*Ag* and MWCNT-MoS_4 as demonstrated in Fig. 14. This reaction reveals that an increase in $\theta_a\left(=\frac{T_\infty}{T_b}\right)$ is proportional to ambient heat, thus, there is heat loss to the ambient which consequently cause the surface temperature to decline. However, the $MWCNT-MoS4$ hybridized nanofluid offers a lower temperature as compared to SWCNT-*Ag* as found in Figs. 13 and 14. Escalating values of thermal radiative term $Ra\left(=\frac{16\sigma_0 T_\infty^3}{3k_f k_a}\right)$ strengthens the thermal field and causes a rise in the temperature as depicted in Fig. 15. The growth in *Ra* causes the mean absorption coefficient to decline thereby raises $\theta(\xi)$. Conversely, rising values of Prandtl number $Pr\left(=\frac{\nu_f(\rho C_p)_f}{k_f}\right)$ created a thinning thermal boundary layer structure (see Fig. 16) and consequently reduces the surface temperature. This fact emanates from a diminished thermal diffusivity as compared to viscous diffusivity with growth in Pr which also aids the

dynamic of heat transfer.

5. Conclusion

The dynamics of flow coupled with heat transport of an elastic deformation in a thermally radiative and convective magneto hybrid single walled carbon nanotube-silver (SWCNT-*Ag*) and multiple walls carbon nanotube-molybdenum tetrasulfide (MWCNT-MoS_4) nanoparticles over a stretchy porous cylinder has been the subject of this study. The investigation is carried out with augmentation of mixed convective hybridized nanofluids under the influence of gravity force, viscous dissipation, nonlinear thermal radiation and slip condition. The controlling mathematical equations are solved by Chebyshev collocation Schemes (CCS) which compared favourably with existing studies under some limiting constraints. The parametric analysis is visualized via different graphs as well as tables depicting the significant contributions of the emerging physical parameters. From the outcomes, the key points are summarily collated as follows.

- There is a reduction in the skin friction coefficient $Cf_xRe^{1/2}$ with escalating values of the slip parameter term γ and the magnetic field term M for both MWCNT-MoS_4 and SWCNT-*Ag* but the converse is the case for a rise in the Eckert number *Ec* and the mixed convection term φ.
- The dynamics of heat transfer across the surface is improved by growing values the mixed convection term φ (0.4, 0.6,1.8) for engine oil base hybridized nanofluid MWCNT-MoS_4 and SWCNT-*Ag*. However, uplifting the thermal radiation *Ra* only improves the Nusselt number $NuRe^{-1/2}$ for MWCNT-MoS_4 while $NuRe^{-1/2}/SWCNT - Ag$ depletes with hike in *Ra* and magnetic field *M*.
- The hydrodynamic boundary structure together with velocity profiles expands with growing values of the stagnation ϵ and volume fractions $\Psi_1 \& \Psi_2$ whereas the trend is reversed for hike in the slip term γ, Darcy *Da* and magnetic field parameter *M* for both hybridized nanofluids.
- Surface temperature distribution is high in the presence of radiation term *Ra*, Eckert number *Ec* and magnetic field term *M* but a reduction in the heat distribution occurs with rising values of the Prandtl number *Pr*, elastic deformation β and the viscoelastic term χ for both SWCNT-*Ag* and MWCNT-MoS_4 hybrid nanofluids.

However, due to its usefulness, further study is encouraged on hybridization of SWCNT-*Ag* and MWCNT-MoS_4 nanofluids flow along a Riga plate in combination with non-Newtonian fluid and activation energy.

Declaration of competing interest

The authors declare that they have no known competing financial interests or personal relationships that could have appeared to influence the work reported in this paper.

Data availability

No data was used for the research described in the article.

References

[1] G. Dharmaiah, F. Mebarek-Oudina, M.S. Kumar, K.C. Kala, Nuclear reactor application on Jeffrey fluid flow with Falkner-skan factor, Brownian and thermophoresis, non linear thermal radiation impacts past a wedge, J. Indian Chem. Soc. 26 (2023), 100907.

[2] S.O. Salawu, E.O. Fatunmbi, S.S. Okoya, MHD heat and mass transport of Maxwell Arrhenius kinetic nanofluid flow over stretching surface with nonlinear variable properties, Res. Chem. 3 (2021), 100125.

[3] W. Jamshed, N.A.A. Mohd Nasir, S.S.P. Mohamed Isa, R. Safdar, F. Shahzad, K. S. Nisar, M.R. Eid, A. Abdel-Aty, I.S. Yahia, Thermal growth in solar water pump using Prandtl-Eyring hybrid nanofluid: a solar energy application, Sci. Rep. 11 (2021), 18704.

[4] H.A. Ogunseye, S.O. Salawu, E.O. Fatunmbi, A numerical study of MHD heat and mass transfer of a reactive Casson-Williamson nanofluid past a vertical moving cylinder, Part. Diff. Eqs. Appl. Math. 4 (2021), 100148.

[5] J.A. Eastman, S.U.S. Choi, S. Li, W. Yu, L.J. Thompson, Anomalously increased effective thermal conductivities of ethylene glycol based nanofluids containing copper nanoparticles, Appl. Phys. Lett. 78 (2001) 718–720.

[6] S.K. Das, N. Putra, P. Thiesen, W. Roetzel, Temperature dependence of thermal conductivity enhancement for nanofluids, ASME J. Heat Transf. 125 (2003) 567–574.

[7] S. Gupta, D. Kumar, J. Singh, MHD mixed convective stagnation point flow and heat transfer of an incompressible nanofluid over an inclined stretching sheet with chemical reaction and radiation, Int. J. Heat Mass Tran. 118 (2018) 378–387.

[8] F.B. Tadesse, O.D. Makinde, L.G. Enyadene, Hydromagnetic stagnation point flow of a magnetite ferrofluid past a convectively heated permeable stretching/shrinking sheet in a DarcyForchheimer porous medium, Sdhan 46 (2021) 115.

[9] W. Jamshed, S. Mishra, P. Pattnaik, K.S. Nisar, S.S.U. Devi, M. Prakash, F. Shahzad, M. Hussain, V. Vijayakumar, Features of entropy optimization on viscous second grade nanofluid streamed with thermal radiation: a Tiwari and Das model Case, Stud. Therm. Eng. 27 (2021), 101291.

[10] A. Shafiq, F. Mebarek-Oudina, T.N. Sindhu, G. Rassoul, Sensitivity analysis for Walters' B nanoliquid flow over a radiative Riga surface by RSM, Sci. Iran. 29 (3) (2022) 1236–1249.

[11] M.D. Shamshuddin, S.O. Salawu, O.A. Beg, A. Kadir, T.A. Beg, Computation of reactive mixed convection radiative viscoelastic nanofluid thermo-solutal transport from a stretching sheet with Joule heating, Int. J. Model. Simulat. 21 (2021) 1–26.

[12] E.O. Fatunmbi, A.T. Adeosun, S.O. Salawu, Entropy analysis of nonlinear radiative Casson nanofluid transport over an electromagnetic actuator with temperature-dependent properties, Part. Diff. Equs. Appl. Math. 4 (2021), 100152.

[13] MdR.B. Mizan, M. Ferdows, M.D. Shamshuddin, O.A. Beg, S.O. Salawu, A. Kadir, Computation of ferromagnetic/nonmagnetic nanofluid flow over a stretching cylinder with induction and curvature effects, Heat Transf. 50 (6) (2021) 5240–5266.

[14] W. Jamshed, S.U. Devi, K.S. Nisar, Single phase based study of Ag-Cu/EO Williamson hybrid nanofluid flow over a stretching surface with shape factor, Phys. Scripta 96 (6) (2021), 065202.

[15] M.H. Esfe, S. Esfandeh, M.H. Kamyab, D. Toghraie, Analysis of rheological behavior of MWCNT-Al_2O_3 (10:90)/5W50 hybrid non-Newtonian nanofluid with considering viscosity as a three-variable function, J. Mol. Liquids 341 (2021), 117375.

[16] M.I. Afridi, I. Tlili, M. Goodarzi, M. Osman, N.A. Khan, Irreversibility analysis of hybrid nanofluid flow over a thin needle with effects of energy dissipation, Symmetry 11 (2019) 663–677.

[17] S.O. Salawu, M.D. Shamshuddin, O.A. Beg, Influence of magnetization, variable viscosity and thermal conductivity on Von Karman swirling flow of H_2O-Fe_3O_4 and H_2O-$Mn - ZnFe_2O_4$ ferromagnetic nanofluids from a spinning DISK: smart spin coating simulation, Mater. Sci. Eng. B 279 (2022), 115659.

[18] N.C. Roy, L.K. Saha, M. Sheikholeslami, Heat transfer of a hybrid nanofluid past a circular cylinder in the presence of thermal radiation and viscous dissipation, AIP Adv. 10 (2020), 095208.

[19] M.S. Khan, S. Mei, Shabnam, U. Fernandez-Gamiz, S. Noeiaghdam, S.A. Shah, A. Khan, Numerical analysis of unsteady hybrid nanofluid flow comprising CNTs-ferrousoxide/water with variable magnetic field, Nanomaterials 12 (2022) 180–199.

[20] H. Waqas, S.M.R.S. Naqvi, M.S. Alqarni, T. Muhammad, Thermal transport in magnetized flow of hybrid nanofluids over a vertical stretching cylinder, Case Stud. Therm. Eng. 27 (2021), 101219.

[21] K. Dhif, F. Mebarek-Oudina, S. Chouf, H. Vaidya, A.J. Chamkha, Thermal analysis of the solar collector cum storage system using a hybrid-nanofluids, J. Nanofluids 10 (4) (2021), 634644.

[22] S.M. Hussain, W. Jamshed, A comparative entropy based analysis of tangent hyperbolic hybrid nanofluid flow: implementing finite difference method, Int. Commun. Heat Mass Tran. 129 (2021), 105671.

[23] S. Shaiq, E.N. Maraj, Z. Iqbal, Remarkable role of $C_3H_8O_2$ on transportation of MoS_2/SiO_2 hybrid nanoparticles influenced by thermal deposition and internal heat generation, J. Phys. Chem. Solid. 126 (2019) 294–303.

[24] I. Chabani, F. Mebarek-Oudina, H. Vaidya, A.I. Ismail, Numerical analysis of magnetic hybrid Nano-fluid natural convective flow in an adjusted porous trapezoidal enclosure, J. Magn. Magn Mater. 564 (2) (2022), 170142.

[25] A.M. Okedoye, S.O. Salawu, E.A. Asibor, A convective MHD double diffusive flow of a binary mixture through an isothermal and porous moving plate with activation energy, Comput. Therm. Sci.: Int. J. 13 (5) (2021) 45–60.

[26] M. Izadi, H.F. Oztop, M.A. Sheremet, S.A.M. Mehryan, N. Abu-Hamdeh, Coupled FHDMHD free convection of a hybrid nanoliquid in an inversed T-shaped enclosure occupied by partitioned porous media, Numer. Heat Transf. Part A Appl. 76 (2019) 479–498.

[27] A.J. Chamkha, I.V. Miroshnichenko, M.A. Sheremet, Numerical analysis of unsteady conjugate natural convection of hybrid water-based nanofluid in a semicircular cavity, J. Therm. Sci. Eng. Appl. 9 (2017), 041004-1041004-9.

[28] N.A. Zainal, R. Nazar, K. Naganthran, I. Pop, MHD mixed convection stagnation point flow of a hybrid nanofluid past a vertical flat plate with convective boundary condition, Chin. J. Phys. 66 (2020) 630–644.

[29] S. Mandal, G.C. Shit, Entropy analysis on unsteady MHD biviscosity nanofluid flow with convective heat transfer in a permeable radiative stretchable rotating disk, Chin. J. Phys. 74 (2021) 239–255.

[30] F. Mebarek Oudina, Convective heat transfer of titania nanofluids of different base fluids in cylindrical annulus with discrete heat source, Heat Tran. Asian Res. 48 (2019) 135–147.
[31] C. Ragavan, S. Munirathinam, M. Govindaraju, A.K. Abdul Hakeem, B. Ganga, Elastic deformation and inclined magnetic field on entropy generation for Walters liquid B fluid over a stretching sheet, J. Appl. Maths. Computat. Mech. 18 (2) (2019) 85–98.
[32] S. Nadeem, N. Abbas, On both MHD and slip effect in micropolar hybrid nanofluid past a circular cylinder under stagnation point region, Can. J. Phys. 97 (4) (2019), 392399.
[33] S.S. Ghadikolaei, K. Hosseinzadeh, M. Hatami, D.D. Ganji, MHD boundary layer analysis for micropolar dusty fluid containing Hybrid nanoparticles (CuAl2O3) over a porous medium, J. Mol. Liq. 268 (2018) 813–823.
[34] K. Hosseinzadeh, A. Asadi, A.R. Mogharrebi, J. Khalesi, S. Mousavisani, D.D. Ganji, Entropy generation analysis of (CH2OH) containing CNTs nanofluid flow under effect of MHD and thermal radiation, Case Stud. Therm. Eng. 14 (2019), 100482.
[35] A.M. Obalalu, Heat and mass transfer in an unsteady squeezed Casson fluid flow with novel thermophysical properties: analytical and numerical solution, Heat Transf. 50 (8) (2021) 7988–8011.
[36] B. Unyong, R. Vadivel, M. Govindaraju, R. Anbuvithya, N. Gunasekaran, Entropy analysis for ethylene glycol hybrid nanofluid flow with elastic deformation, radiation, non-uniform heat generation/absorption, and inclined Lorentz force effects, Case Stud. Therm. Eng. 30 (2022), 101639.
[37] P. Kameswaran, M. Narayana, P. Sibanda, P. Murthy, Hydromagnetic nanofluid flow due to a stretching or shrinking sheet with viscous dissipation and chemical reaction effects, Int. J. Heat Mass Tran. 55 (2526) (2012), 75877595.